Volume 1 | Number 1 | Jan 2013 | Pages 1–100

Journal of
Materials Chemistry B

Materials for biology and medicine
www.rsc.org/materialsB

ROYAL SOCIETY
OF CHEMISTRY

ROYAL SOCIETY
OF CHEMISTRY

www.rsc.org/materialsB

Study on effects of naphthalimide derivative-capped quantum dots on the cellular internalization, proliferation, and apoptosis ability

Mei-Xia Zhao*, Er-Zao Zeng, Yang Li, and Chao-Jie Wang*

Naphthalimide derivative-capped QDs effectively inhibited the proliferation of cells due to apoptosis via a ROS mediated mitochondrial dysfunction.
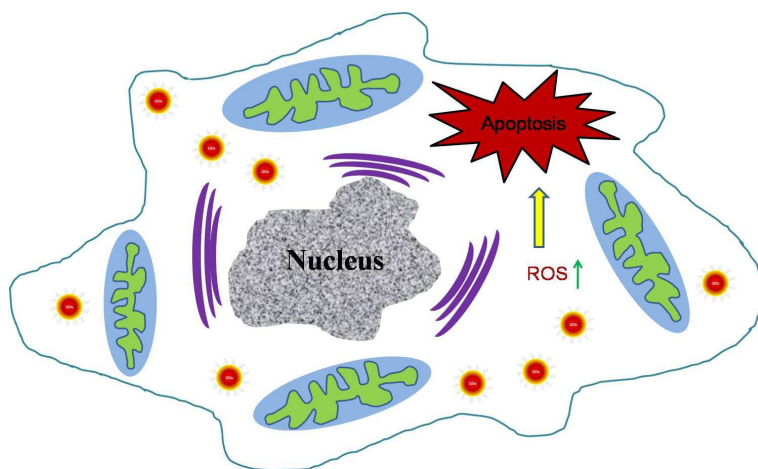
PAPER

Study on effects of naphthalimide derivative-capped quantum dots on the cellular internalization, proliferation, and apoptosis ability

Mei-Xia Zhao*, Er-Zao Zeng, Yang Li and Chao-Jie Wang*

Quantum dots (QDs) have shown great potential in monitoring and imaging cancer cells because of their unique photochemical and photophysical properties. However, it is little-known if QDs affect the cellular internalization, proliferation and apoptosis. Here a new class of multifunctional QDs capped with ligands that possess an L-Lys or L-Arg and a naphthalimide (NI), linked by carboxyl groups (L-Lys-NI@QDs

10 and L-Arg-NI@QDs, respectively), have been synthesized. We found that these QDs are of controllable sizes, in the range of 4 to 5 nm and have strong optical emission properties. The cellular uptake of naphthalimide derivative-capped QDs was monitored by flow cytometry and confocal microscopy. The results of in vitro cytotoxicity revealed that naphthalimide derivative-capped QDs, with better cell selectivity, could inhibit the growth of multiple cancer cells more potently than amonafide. They

15 effectively inhibited the proliferation of cells due to apoptosis, which confirmed by Hoechst 33342, annexin V-FITC and JC-1 staining and MMP experiments. The most potent naphthalimide derivative-capped QDs, L-Arg-NI@CdSe/ZnS, were verified to efficiently induce apoptosis via a reactive oxygen species (ROS) mediateing mitochondrial dysfunction, and were more effective in promoting programmed cell death in HepG2 cells in a preliminary mechanistic study.

Introduction

20 In recent years, research on quantum dots (QDs) has generated numerous biological applications due to the unique electrochemical and photophysical properties they provide.[1-5] Although issues regarding the cytotoxicity of QDs have been

25 raised,[6,7] recent studies suggested that the surface coatings of QDs could decrease their toxicity.[8,9] Therefore, when interfaced with biological molecules including proteins, peptides, carbohydrates, and DNA, the resulting QD-biocomposites have widespread applicability in areas ranging from cellular

30 fluorescence imaging,[10,11] in vivo fluorescence imaging[12,13] and diagnostics in biomedicine to environmental monitoring for public health and security.[14,15] One of the major hurdles in the use of QD nanoparticles for in vivo applications is the delivery and organelle-specific targeting of QDs.

35 Naphthalimide architectures have been evaluated extensively as antitumor agents and a class of desirable pharmacophores due to the wide bioactivities.[16,17] However, many naphthalimides in clinical trials were abandoned because of their various adverse effects.[18] The modification of side chain or the substituents on the

40 ring have been attempted to reduce the adverse effects and improve the potency.[19] Recent studies confirmed that the naphthalimide modified with both spermidine and homospermidine have enhanced cytotoxicity to cancer cells over the normal cells in vitro, and induced B16 cell apoptosis.[20]

45 Apoptosis is a highly regulated process that plays a crucial role in

the maintenance of cellular homeostasis in the adult and in the pathology of a variety of diseases.[21] Apoptosis can be characterized by a variety of morphological features such as membrane blebbing, cell shrinkage, condensation of the

50 cytoplasm, and internucleosomal cleavage of DNA.[22,23] Understanding processes underlying apoptosis will help to find new targets for drug development and curing diseases. And the measurement of apoptosis will help us to find an early indicator for the therapeutic interventions and then to enhance curable

55 possibilities to associated diseases.[24,25] Therefore, the development of this simple and convenient approach to apoptosis detection has received more and more interest.

Here, we synthesized a new class of multifunctional QDs (L-Lys-NI@QDs and L-Arg-NI@QDs) with controllable sizes and

60 strong optical emission properties. And we compared their biological activity using MTT assay with HepG2, QSG-7701, and HeLa cells. The results revealed that these QDs have higher inhibition ratio to multiple cancer cells, compared with amonafide. The increased inhibition ratio was due to apoptosis as

65 confirmed by annexin V-FITC and Hoechst 33342 staining, mitochondrial membrane potential (MMP) and ROS experiments analysed by flow cytometry and confocal microscopy. Compared with L-Lys, L-Arg with higher positive charge resulted in a considerable increase in the intracellular uptake of QDs.[26]

70 Moreover, L-Arg contribute to enhancing the cellular membrane permeability of many biologically active molecules, such as drugs, peptides, etc.[27,28] So our results revealed that many more L-Arg-NI@CdSe/ZnS QDs were accumulated in the cancer cells

This journal is © The Royal Society of Chemistry 2013

J. Mater. Chem. B, 2014, **[vol]**, 00–00 | 1

than other QDs. And ROS level increased in cancer cells treated with QDs, suggesting that QDs may trigger cell apoptosis via ROS generation mediated mitochondrial dysfunction.

Experimental section

1. Materials

Unless specified, chemicals were purchased from Sigma-Aldrich (St. Louis, MO) and used without further purification. Foetal bovine serum (FBS) and RPMI-1640 media were from Invitrogen Corporation. All organic solvents were purchased from EM Sciences. HeLa (human cervical carcinoma cell), HepG2 (human hepatocellular liver carcinoma cells), and QSG-7701 (human normal hepatocyte) cells were purchased from Shanghai Institute for Biological Science, Chinese Academy of Science (Shanghai, China).

2. Apparatus

^{1}H NMR spectra were recorded on a Bruker AV-400 model spectrometer. ESI-MS spectra were recorded on a Thremo LCQ-DECA-XP spectrometer. UV-Vis absorption spectra were acquired with a Varian Cary 300 BIO UV-Vis spectrophotometer equipped with a temperature controller ($\pm$ 0.1 K). The fluorescence spectra were measured by using a Cary Eclipse Fluorescence Spectrophotometer (American, Agilent, Co.). The fluorescence quantum yields (QYs) were calculated by using organic dyes with known QY as the standard, the PL QY data reported here were obtained by using rhodamine B (RhB) as the standard (QY = 89 %).[29] The transmission electron micrographs (TEM) were taken on a JEOL JEM-200CX transmission electron microscope, employing an accelerating voltage of 200 kV. The cell fluorescence intensity was analysed by a FACSCalibur flow cytometer (Becton Dickinson & Co., Franklin Lakes, NJ). Confocal microscopy images were obtained with a confocal laser scanning fluorescence microscope (Leica SP8).

3. Synthesis of N-(4-bromobutyl)-1,8-naphthalimide

1,8-Naphthalimide (1.97 g, 10.0 mmol), anhydrous K_2CO_3 (4.14 g, 30.0 mmol), KI (0.25 g, 1.5 mmol), hexadecyl trimethyl ammonium bromide (1.20 g, 3.3 mmol) and 50 mL acetone were placed in a round-bottomed flask with a magnetic stirrer, and 1,4-dibromobutane (6.48 g, 30.0 mmol) were added slowly. The solution reacted at room temperature with constant stirring for 3 d, and the reaction process was monitored by TLC. After completion, the precipitate was filtered and the removal of the solvent resulted in a solid which was subjected to column chromatography using petroleum ether/ethyl acetate mixture as the eluent to yield the compounds N-(4-bromobutyl)-1,8-naphthalimide. Yield 85.3%, pale yellow solid. ^{1}H NMR (400 MHz, CDCl$_3$) δ: 8.6l (d, 2H); 8.23(d, 2H); 7.77 (t, 2H); 4.24 (t, 2H); 3.48 (t, 2H); 1.89-1.99 (m, 4H).

4. Synthesis of Boc-L-Lys and Boc-L-Arg

L-Lys (1.46 g, 10 mmol) or L-Arg (1.74 g, 10 mmol) was dissolved in a small amount of water (about 4.0 mL), and 2.0 mL NaHCO$_3$ saturated solution was added. After the solution was cooled 0 ℃, di-tert-butyl dicarbonate ester ((BOC)$_2$O) (0.88 g, 4.0 mmol) was added and reacted for 1 h with constant stirring. Then the solution was heated to 25 ℃ with constant stirring for 12 h. After reaction finished, 10.0 mL of water was added and the compound was extracted with chloroform. The aqueous phase was adjusted to alkaline with saturated NaHCO$_3$ solution and extracted with chloroform. Removal of the solvent in aqueous phase resulted in a solid. After vacuum drying, a slightly yellowish solid was obtained.

Data for Boc-L-Lys: yield 89.5%; The ^{1}H NMR δ: 3.16-3.19 (t, 1H); 2.76-2.80 (t, 2H); 1.46-1.54 (m, 6H); 1.27 (s, 9H).

Data for Boc-L-Arg: yield 86.3%; The ^{1}H NMR δ: 3.18-3.22 (t, 1H); 2.66-2.71 (t, 2H); 1.55-1.62 (m, 4H); 1.41 (s, 9H).

5. Synthesis of L-Lys-butyl-1,8-naphthalimide (L-Lys-NI) and L-Arg-butyl-1,8-naphthalimide (L-Arg-NI)

Boc-L-Lys (2.46 g, 10.0 mmol) or Boc-L-Arg (2.73 g, 10.0 mmol) and K_2CO_3 (2.07 g, 10.0 mmol) were dissolved in dimethyl sulfoxide (DMSO) solution, and the solution was stirred at room temperature (25 ℃) for 15 min. After the addition of N-(4-bromobutyl)-1,8-naphthalimide (3.32 g, 10.0 mmol), the solution was heated to 45 ℃ with constant stirring for 12 h. After completion of the reaction, the precipitate was filtrated getting a light yellow filtrate. Then 30 mL of water was added to the filtrate, and the precipitate was filtrated to yield the yellow compounds. Then the compounds was dissolved in 100 mL methyl alcohol solution, and (BOC)$_2$O (2.18 g, 10.0 mmol) was added. Then the solution was stirred at room temperature (25 ℃) for 12 h. After completion, the reaction mixture was evaporated to dryness under reduced pressure, and the residues were purified by silica gel column chromatography using CH_2Cl_2/CH_3OH mixture as the eluent to obtain the BOC protected intermediates Boc-L-Lys (or Boc-L-Arg).

Then the BOC protected intermediates Boc-L-Lys (or Boc-L-Arg) (5.0 mmol) was dissolved in 20 mL ethanol, and stirred at 0 ℃ for 10 min. Then 4 M HCl was added dropwise at 0 ℃. The reaction mixture was stirred at room temperature overnight. The solution typically gave a white solid precipitate. The solid was filtered, washed several times with absolute ethanol, and dried under vacuum to give the pure target compounds **L-Lys-NI** and **L-Arg-NI**.

L-Lys-butyl-1,8-naphthalimide (L-Lys-NI): Yield 65.4%, yellowish solid; Mass spectrometry (MS) (electrospray ionization (ESI)), m/z: 397.4 [M+H]; ^{1}H NMR (400 MHz, D$_2$O)δ: 8.24 (s, 1H), 7.70-7.93 (m, 4H), 7.20-7.43 (m, 2H), 3.42-3.55 (m, 4H), 2.85-2.92 (m, 8H), 2.70-2.83 (m, 8H).

L-Arg-butyl-1,8-naphthalimide (L-Arg-NI): Yield 61.5%, yellowish solid; MS-ESI, m/z:425.5 [M+H]; ^{1}H NMR (400 MHz, D$_2$O)δ: 8.44-8.49 (m, 4H), 7.84-7.88 (t, 2H), 4.03-4.06 (t, 1H), 3.39-3.44 (m, 6H), 2.49-2.50 (m, 4H), 1.64-1.68 (m, 2H), 1.45-1.49 (m, 2H).

6. Synthesis of quantum dots (QDs)

CdSe, CdSe/CdS and CdSe/ZnS QDs capped with tri-n-trioctylphosphine oxide (TOPO) were synthesized using organometallic procedures as previously reported.[30] The as-prepared CdSe, CdSe/CdS and CdSe/ZnS QDs using this procedure were found to show high crystallinity and high quantum yields (~43.2 %, ~58.6 % and ~79.4 %, respectively), narrow emission spectra (FWHM ~28, ~31 and ~36 nm, respectively), and narrow size distributions (~3.4, ~4.2 and ~3.9 nm, respectively).

7. Synthesis of water-soluble naphthalimide derivative-capped QDs nanoparticles (L-Lys-NI@QDs and L-Arg-NI@QDs)

The syntheses of water-soluble naphthalimide derivative-capped QDs were made by surface modification of the QDs as described previously reported with some slight modification.[31] The TOPO ligands on the solubilised QDs were replaced with naphthalimide derivative through the carboxyl group by ultrasonic method. The mixture QDs in chloroform solution and naphthalimide derivative in N, N-dimethylformamide was sonicated for 4 h. Then, ethyl acetate was added to precipitate the nanocrystal complexes to purify the nanocrystals from side products and unreacted precursors. The purified nanocrystal complexes could be dissolved in water or other various aqueous media.

8. Cell culture

HepG2 (human hepatocellular liver carcinoma), QSG-7701 (humans normal liver), and HeLa (Human cervical carcinoma) cells were cultured in RMPI-1640 medium supplemented with heat-inactivated FBS (10 % v/v) and 1% (v/v) penicillin-streptomycin (100 U/mL penicillin G and 100 mg mL^{-1} streptomycin) at 37 ℃ under a 5% CO_2 atmosphere. Cells were counted by hemocytometer and seeded in 96-well microplate at a density of 5×10^4 cells/well.

9. Cell viability assays

The antitumor ability of complexes was evaluated in HepG2, QSG-7701 and HeLa cells by the conversion of 3-(4,5-dimethyl-2-thiazolyl)-2,5-diphenyltetrazolium bromide (MTT) to a purple formazan precipitate as previously described.[32] Briefly, cells were seeded into 96-well plates at 5×10^4 cells/well. After 12 h, various concentrations (1, 2, 5, 10, 20, and 40 μM) of samples were subsequently added and incubated for 48 h (the concentrations of original QDs was 0.05, 0.1, 0.2, 0.4, 0.8 and 1.0 μM). Then 20 μL MTT (2.5 mg mL^{-1}) was added to each well. After 4 h incubation, the medium was then removed and 100 μL DMSO was added to the plates to dissolve the formazan products. The absorbance of the solution containing the extracts was read at 570 nm on a Tecan Infinite F200 M200 multimode plate reader. The inhibition rate was calculated from plotted results using untreated cells as 100%.

10. Cellular uptake of targeted QDs

HepG2, QSG-7701, and HeLa cells seeded in 6-well tissue culture plate (Corning) were incubated with original QDs, and naphthalimide derivative-capped QDs at 37 ℃. After incubation for 12 h, the cells were thoroughly washed with PBS buffer at pH 7.4. Then cells were trypsinised and washed twice with PBS buffer. The cells were analysed by a FACSCalibur flow cytometer (Becton Dickinson & Co., Franklin Lakes, NJ) immediately under excitation at 488 nm and emission at (580 ± 20) nm.

For fluorescence microscopy observation of samples after treatment of cells for 12 h, the cells were washed with PBS and incubated with Hoechst 33342 (10 μg mL^{-1}) for 30 min at 37 ℃, then viewed with a confocal microscope (Leica-SP8). The samples were excited at 488 nm with an Ar laser. A band-pass from 580 to 650 nm was adopted for observation. Cell nuclei stained with Hoechst 33342 solution were observed under an emission of 405 nm, and analysed from 430 to 480 nm.

11. Apoptosis assay. Hoechst staining

Cells were seeded in a 35 mm diameter culture dish containing 15 mm diameter glass cover-slips and allowed to adhere overnight. At the indicated time point (12, 24, 48 h) following treatment with the naphthalimide derivatives, original QDs, and naphthalimide derivative-capped QDs, cells were stained with Hoechst 33342 (10 μg mL^{-1}) for 30 min at 37 ℃ and imaged using confocal microscope (Leica-SP8). The rate of abnormal (condensed or fragmented) nucleus was obtained by counting in eight randomly chosen fields per dish; per experimental group from three separate experiments and expressed as a percentage of apoptotic nucleus compared to total number of cells. Cell nuclei stained with Hoechst 33342 were observed under an emission of 405 nm, and analysed from 430 to 480 nm.

12. Annexin V staining study of cell prophase apoptosis

Cell prophase apoptosis was evaluated by annexin V-FITC apoptosis detection kit using FACSCalibur flow cytometer analysis and confocal microscope. Briefly, the HepG2 cells were seeded in 6-well plates. After 24 h, this medium was replaced with medium containing samples. After 6 h treatment with samples (3 μM), cells were washed with PBS and resuspended in PBS buffer. Then cells were incubated with annexin V for 10 min at 37 ℃ and were passed through a FACSCalibur flow cytometer (Becton Dickinson & Co., Franklin Lakes, NJ). Data were analysed by using BD Cell Quest software. Percentages of live and apoptotic cells were determined on the basis of negative controls obtained by staining controls only with PI or only with annexin V.

For fluorescence microscopy observation, cells were seeded in a 35 mm diameter culture dish containing 15 mm diameter glass cover-slips. After treatment with samples for 6 h, the cells were washed with PBS and incubated with annexin V for 10 min at 37 ℃, then viewed with a confocal microscope (Leica-SP8). The excitation wavelength for green annexin V was 488 nm, and the band path for the marker imaging was from 500 to 560 nm.

13. Cell cycle analysis

HepG2 cells were seeded into 6-well plates and incubated for 24 h. Samples were then added into the wells and incubated for 48 h. All the cells, including the floating cells in the culture medium, were harvested by trypsinisation, washed twice with PBS and fixed with aqueous ethanol (70 % v/v) at -20 ℃ at least 12 h. The cells were centrifuged and washed twice with ice-cold PBS. To ensure DNA staining, cells were resuspended and treated with DNase free RNase (100 μg mL^{-1}) for 30 min at 37 ℃. After RNase treatment, propidium iodide (PI) (10 μg mL^{-1}) was added and incubated for 30 min in the dark at 37 ℃. Cells were finally washed with PBS, resuspended in 0.5 mL PBS and measured by a FACSCalibur flow cytometer. 10 000 Events were acquired and the experiments were repeated at least three times.

14. Analysis of mitochondrial membrane potential

We incubated HepG2 cells with samples for 24 h at 37 ℃. The cells were incubated at 37 ℃ in suspension with media containing 10 μg mL^{-1} JC-1 (5,5′, 6,6′-tetrachloro-1,1′, 3,3′-tetraethylbenzimidazolylcarbo-cyanine iodide; Molecular Probes)

This journal is © The Royal Society of Chemistry 2014

J. Mater. Chem. B, 2014, **[vol]**, 00–00 | 3
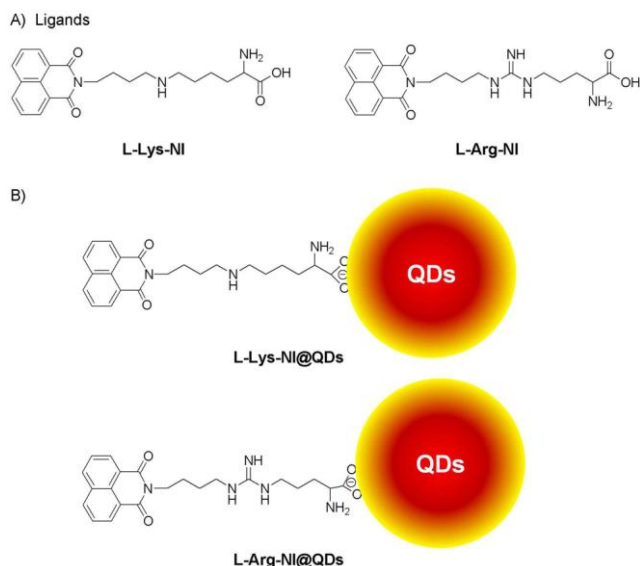
Scheme 1 (A) Ligand structures and (B) schematic illustration of the naphthalimide derivative-capped QDs in this report.

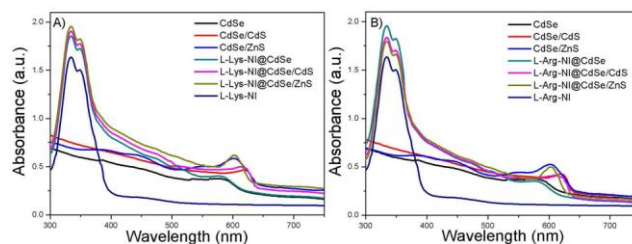for 10 min. The cells subsequently subjected with a FACSCalibur
5 flow cytometer. Mitochondria in which the mitochondrial membrane potential is accumulated so-called J-aggregates that fluoresces red, whereas those with a collapsed membrane potential fluoresces green. We calculated the mitochondrial membrane potential for single cells by dividing the intensity of
10 the 590 nm (red) with its corresponding 530 nm (green). 10 000 events were acquired for each samples, and red and green mean fluorescence intensities were analysed by using BD Cell Quest software.

For fluorescence microscopy observation, cells seeded in a 35
15 mm diameter dish containing 15 mm diameter glass cover-slips were incubated for 10 min in 10 μg mL^{-1} JC-1, and viewed using confocal microscopy (Leica-SP8). We calculated the mitochondrial membrane potential by dividing the intensity of the 590 nm (red) images with its corresponding 530 nm (green)
20 images.

15. Measurement of ROS

Accumulation of intracellular reactive oxygen species (ROS) was determined using the 2′,7′-dichlorofluorescein diacetate (H$_2$DCF-DA) as previously described. In details, after 6 h treatment with
25 samples, the cells were rinsed three times with PBS to remove unbound samples. The cells were incubated with 10 μM of H$_2$DCF-DA at 37 ℃ for 30 min, and washed twice with PBS after incubation. Following this, the fluorescence intensity of cells was measured immediately with excitation at 488 nm and
30 emission at 530 nm by a FACSCalibur flow cytometer and confocal microscopy.

Results and discussion

1. Preparation and characterisation of naphthalimide derivative-capped QDs nanoparticles

35 In this work, three QDs (CdSe, CdSe/CdS and CdSe/ZnS) were used as precursors of the naphthalimide derivative-capped QDs (Scheme 1). The water-soluble naphthalimide derivative-capped QDs were prepared by the solution-phase synthesis method. Fig.

40 **Fig. 1** UV-vis spectra of (A) L-Lys-NI-capped QDs in PBS buffer and original QDs in chloroform solution, and (B) L-Arg-NI-capped QDs in PBS buffer and original QDs in chloroform solution.
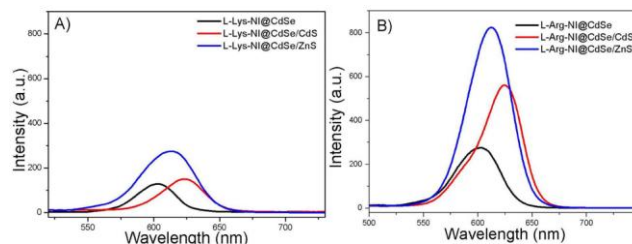

Fig. 2 Fluorescence spectra of (A) L-Lys-NI-capped QDs and (B) L-Arg-
45 NI-capped QDs in PBS buffer.

1 depicts the absorption spectra of QDs and two naphthalimide derivative-capped QDs (L-Lys-NI-capped QDs and L-Arg-NI-capped QDs). We can see that the UV-vis absorption spectra of naphthalimide derivative-capped QDs exhibit a new absorption
50 band at 310 to 350 nm with the addition of L-Lys-NI and L-Arg-NI, where the naphthalimide absorbs. And there was no too much difference in the position or width of absorbance bands from hydrophobic QDs, suggesting that naphthalimide derivatives have been successfully incorporated into QDs nanoparticles.

55 The naphthalimide derivative-capped QDs were further characterized by fluorescence spectroscopy. Fig. 2 shows the emission spectra of L-Lys-NI-capped QDs and L-Arg-NI-capped QDs. The fluorescence peak of naphthalimide derivative-capped QDs exhibit a slightly red-shifted emission compared with that of
60 corresponding QDs, suggesting that the emission arises due to the recombination of naphthalimide derivative on surface of QDs. The quantum yields (QYs) of QDs followed the order L-Arg-NI@CdSe/ZnS (~70.6%) > L-Arg-NI@CdSe/CdS (~50.1%) > L-Lys-NI@CdSe/ZnS (~41.8%) > L-Arg-NI@CdSe (~40.6%) > L-
65 Lys-NI@CdSe/CdS (~28.4%) > L-Lys-NI@CdSe (~20.3%). The positive charge located on the QDs surface may prevent the aggregation of the QDs by strong repellent forces among particles.[33] At the same time, the positive charge of the L-Arg was even higher than that of L-Lys. So the fluorescence intensity
70 of the L-Arg-NI-capped QDs was stronger compared with that of L-Lys-NI-capped QDs. In addition, TEM images (Figs. S1 and S2 in the ESI†) showed that the naphthalimide derivative-capped QDs maintained the very similar good dispersive, uniform size of 4-5 nm in diameter.

75 #### 2. Cellular uptake of naphthalimide derivative-capped QDs nanoparticles

The cellular uptake properties of QDs are important factors that can influence their antiproliferative activity. The cellular uptake properties of original QDs and naphthalimide derivative-capped
80 QDs can be studied by flow cytometry and confocal microscopy. To study the uptake and intracellular localization of original QDs and naphthalimide derivative-capped QDs, the tumorous HepG2,

HeLa cells and normal QSG-7701 cells were incubated with original QDs and naphthalimide derivative-capped QDs for 12 h. Firstly, flow cytometry was used to obtain semiquantitative data on the uptake of QDs into cells (Fig. 3). Cells not treated with QDs with negligible background luminescence were used as control. The intracellular intensity of fluorescent L-Arg-NI@CdSe/ZnS QDs in two cancer cells (Fig. 3A, B) was found to be significantly enhanced compared to that of normal cells (Fig. 3C) under the same conditions. On the basis of the flow cytometry values, the average fluorescence intensity of HepG2 cells (Fig. 3A) was increased by thirty-six times (11642 to 322), while the average fluorescence intensity of QSG-7701 cells (Fig. 3C) only increased fifteen times (4927 to 328). However, the intracellular intensity of fluorescent CdSe/ZnS QDs in two cancer cells (Fig. 3D, E) was similar to that of normal cells (Fig. 3F) under the same conditions. At the same time, the intracellular intensity of fluorescent CdSe/ZnS QDs in three cells was found no obvious enhancement. It confirmed that the internalization of naphthalimide derivative-capped QDs were more efficient in cancer cells compared to their normal counterparts.

Flow cytometry cannot be discriminated among membrane-associated, cytoplasmic, and nuclear localization, while the cellular distribution of original QDs and naphthalimide derivative-capped QDs can be studied by confocal microscopy. The confocal images of HepG2, HeLa, and QSG-7701 cells treated with L-Arg-NI@CdSe/ZnS under identical conditions are shown in Fig. 4. It was apparent that a substantial intracellular uptake of the QDs took place in HepG2 and HeLa cancer cells compared with QSG-7701 cells under the same conditions. And the fluorescence emitted from QDs distributed mostly in the cytoplasm, which agrees well with the previous study in the literature.[34] However, there was no obvious accumulation of CdSe/ZnS QDs particles in three kinds of cells under the same conditions (Fig. S3 in the ESI†). The results suggested that many more naphthalimide derivative-capped QDs were accumulated in cancer cells, which is consistent with the results of flow cytometry. This internalization of naphthalimide derivative-capped QDs may have a significant effect on the biological behaviour of the target cancer cells.

3. Cell cytotoxicity assay

To explore the cell toxicity of the naphthalimide derivatives, original QDs, and naphthalimide derivative-capped QDs nanoparticles, HepG2, QSG-7701, and HeLa cells were treated with different concentrations of samples for 48 h, and cell toxicity was determined by the MTT assay. And amonafide, naphthalimide derivatives, and original QDs was used as control. The IC_{50} values of the samples on the growth of several types of cells were shown in Table S1 in the ESI†. On the basis of IC_{50} values, the order of cell toxicity of the naphthalimide derivative-capped QDs is: L-Lys-NI@CdSe > L-Lys-NI@CdSe/CdS > L-Arg-NI@CdSe > L-Lys-NI@CdSe/ZnS > L-Arg-NI@CdSe/CdS > L-Arg-NI@CdSe/ZnS > amonafide. Notably, all the naphthalimide derivative-capped QDs have less cell toxicity on the normal liver QSG-7701 cells than on another two types of cancer cells. Interestingly, the L-Arg-NI@CdSe/ZnS QDs is more potent than amonafide against all the cells screened (approximately 9-fold more potent than amonafide in killing HepG2 cells), while its cell toxicity against the normal liver cells, QSG-7701 (IC_{50} values about 35.26 μM), is only slightly higher than that of amonafide (IC_{50} values about 38.57 μM). However,
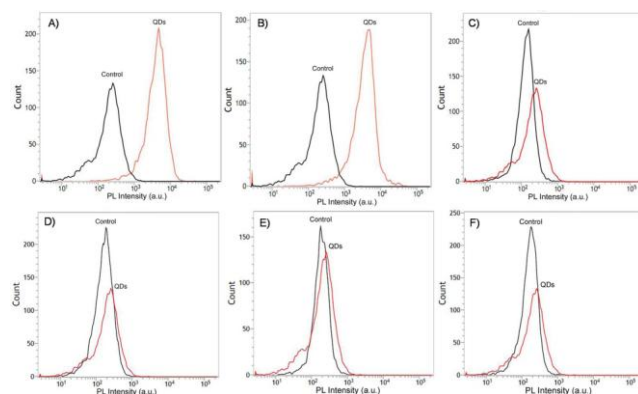

Fig. 3 The flow cytometry data of (A) HepG2, (B) HeLa, (C) QSG-7701 cells loaded with L-Arg-NI@CdSe/ZnS and (D) HepG2, (E) HeLa, (F) QSG-7701 cells loaded with CdSe/ZnS under identical conditions.
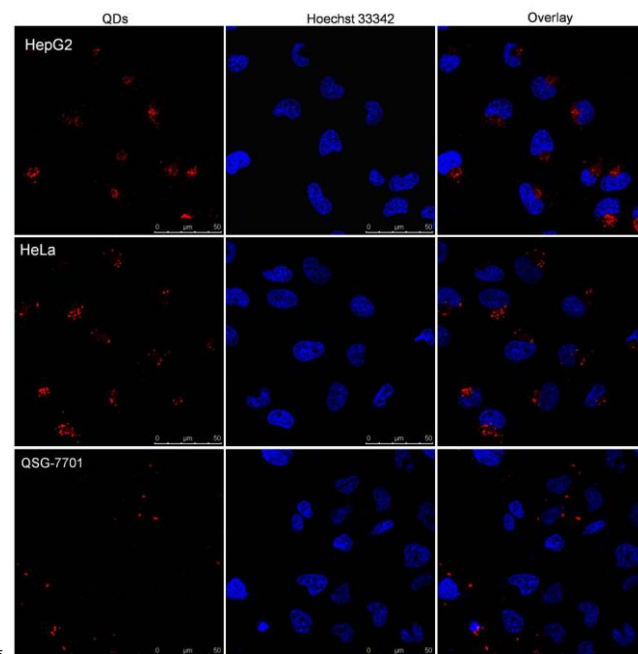

Fig. 4 Confocal images of living cells (HepG2, HeLa, and QSG-7701) loaded with L-Arg-NI@CdSe/ZnS under identical conditions. L-Arg-NI@CdSe/ZnS QDs solution (3 μM) were used and incubated with the cells at 37 ℃ for 12 h. In all cases, blue represents emission from Hoechst 33342 and red represents emission from QDs.

the cell toxicity of original QDs is higher in three types of cells, and it is not obvious selective for normal cells and cancer cells. At the same time, the cell toxicity of naphthalimide derivatives is lower for normal cells and cancer cells. These results suggeste that the naphthalimide derivative-capped QDs can kill tumor cells with less damage to normal cells.

4. Induction of apoptosis

Apoptosis is a programmed or suicidal cell death, which plays an important role in maintaining balance between cell proliferation and death. To evaluate the morphologic characteristics of apoptotic nuclei, the cells were stained with Hoechst 33342 after incubation with naphthalimide derivatives, original QDs, naphthalimide derivative-capped QDs and amonafide for the indicated times and investigated using confocal microscopy. Representative images of the cells treated with samples are
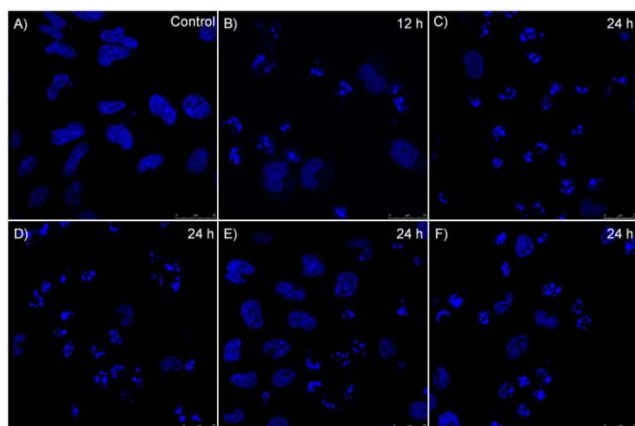
This journal is © The Royal Society of Chemistry 2014

J. Mater. Chem. B, 2014, **[vol]**, 00–00 | **5**

Fig. 5 Morphological changes were examined by Hoechst 33342 staining and observed with a confocal microscope. HepG2 cells were treated with L-Arg-NI@CdSe/ZnS QDs (3 µM) for A) control, B) 12 h, and C) 24 h; D) HeLa, and E) QSG-7701 cells were treated with L-Arg-NI@CdSe/ZnS QDs for 24 h; F) HepG2 cells were treated with amonafide (25 µM) for 24 h.

shown in Fig. 5. Control cells exhibit homogeneous and intact nuclear staining, and apoptotic cells in HepG2 (Fig. 5B,C) and HeLa (Fig. 5D) cells increase gradually in a time-dependent manner and display typical apoptotic changes, such as stained brightness, reduction of cellular volume, fragmented nuclei, and condensed chromatin, etc. But QSG-7701 cells treated with QDs show no obvious apoptosis (Fig. 5E), and amonafide has a little apoptosis-inducing effect on HepG2 cells (Fig. 5F). The images of the cells treated with naphthalimide derivatives and original QDs are shown in Fig. S4 in the ESI†. It can be found that the naphthalimide derivatives can hardly induce apoptosis. And the original QDs have a little apoptosis-inducing effect on HepG2 cells. It perhaps resulted from the substantial intracellular uptake of the naphthalimide derivative-capped QDs in cancer cells compared with normal cells under the same conditions. Because the apoptosis induced by naphthalimide derivatives and original QDs is not obvious, they are not to explore in following experiments.

It is well known that cells in the early stages of apoptosis can be distinguished from necrotic cells by their ability to be labeled with annexin V. Annexin V could bind to the membrane
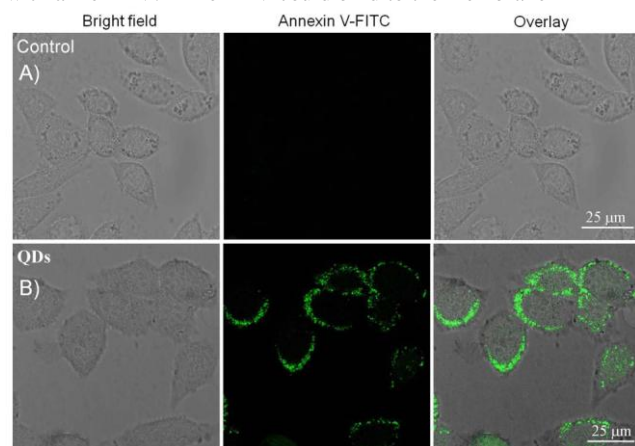

Fig. 6 Representative confocal images of HepG2 cells: A) control, B) after treatment with L-Arg-NI@CdSe/ZnS QDs (3 µM) for 6 h. Cells were stained green with annexinV-FITC (excitation at 488 nm and emission at 500-560 nm).
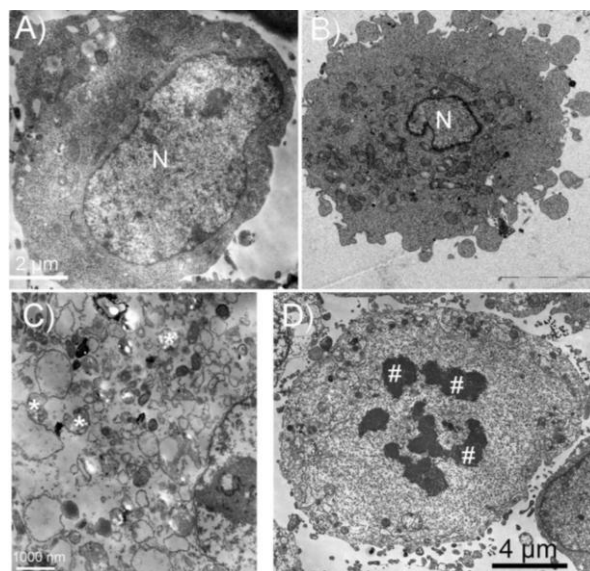

Fig. 7 Representative TEM images of HepG2 cells: A) control, B)-D) after treatment with L-Arg-NI@CdSe/ZnS QDs (3 µM) for 48 h. Normal HepG2 cells are round and their surface is covered with microvilli projecting in all directions (A); in apoptotic cells the nucleus is shrinked (N), the mitochondria are swollen and unstructured (*), and the chromatin is condensed(#; B-D).

phospholipid phosphatidylserine (PS), which is externalized from the inner to the outer surface of the plasma membrane in the early stage of apoptosis.[35] Thus, we investigated the potential of naphthalimide derivative-capped QDs to identify apoptotic cells from living cells by annexin V-FITC staining assays. The images in Fig. 6 show that there were no obvious apoptosis-related phenomena of control cells. However, the cell membrane had obvious green fluorescence of annexin V-FITC in HepG2 cells treated with L-Arg-NI@CdSe/ZnS QDs. This behaviour is a strong indicator of early stage apoptosis. It is well-known that the visual field of confocal microscopy is small, which only confirmed the occurrence of apoptosis, but flow cytometry could offer rapid and sensitive measurements of apoptosis and confirm the number of apoptosis more exactly. So we further explored the stages of apoptosis by flow cytometry. The results of flow cytometry are shown in Fig. S5 in the ESI†. Compared with control cells (where the percentage of apoptosis was about 9.8%), the percentage of apoptosis was about 69.2% after treatment with L-Arg-NI@CdSe/ZnS QDs. The percentage of apoptosis of HepG2 cells treated with amonafide was about 48.3%. The significant number of apoptosis suggests that cells treated with naphthalimide derivative-capped QDs underwent apoptosis.

On the basis of the above studies, we further explored the apoptosis behaviour of naphthalimide derivative-capped QDs on the HepG2 cells using TEM. TEM is the most convincing method for the analysis of apoptosis. Fig. 7 shows the images of the cells in the control group and the ones treated with QDs. The morphology of the cells in the control group is preserved normal and its surface is covered with the uniform chromatin in all directions (Fig. 7A). However, the cells treated with L-Arg-NI@CdSe/ZnS QDs show the obvious features of apoptosis. As shown in Fig. 7B-D, the nucleus is shrinked (N) (Fig. 7B), the mitochondria are swollen and unstructured (Fig. 7C), and the chromatin is condensed (Fig. 7D) in apoptosis of HepG2 cells.

This provides strong evidence that naphthalimide derivative-capped QDs can induce apoptosis in cancer cells.

5. Flow cytometric analysis of cell cycle

The HepG2 cells treated with naphthalimide derivative-capped QDs revealed the apoptosis-related phenomena, such as decrease of viability, shrinkage in morphology, condensation of chromatin, etc. To further investigate the results of the above observed arrest, quantitation of sub-G1 DNA content after PI staining and flow cytometry analysis was performed for demonstration of apoptosis. Fig. 8 shows the effect of samples on cell cycle in PI stained HepG2 cells after QDs treatment for 48 h. The flow cytometric data of cell cycle, after L-Arg-NI@CdSe/ZnS QDs treatment of HepG2 cells, revealed that there was significant increase in DNA content in the sub-G1 phase ($61.3 \pm 1.2\%$) compared to the control cells ($50.4 \pm 1.1\%$), but DNA content decreased in S phase ($19.5 \pm 0.6\%$) compared to untreated control cell ($30.7 \pm 0.9\%$). And the most of the cells treated with L-Arg-NI@CdSe/ZnS QDs ($66.2 \pm 1.9\%$) have undergone apoptosis. However, amonafide ($25 \ \square \ M$) caused a little apoptosis ($41.7 \ \square \ 1.2\%$). These data provided the information that naphthalimide
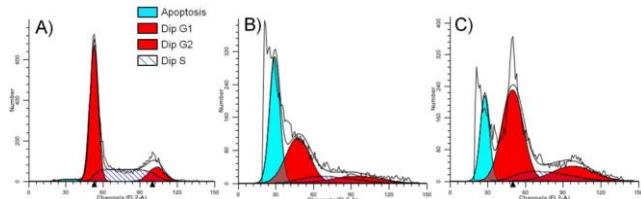

Fig. 8 Quantitative cell cycle in different phase distribution results for HepG2 cells after treatment with QDs and amonafide for 48 h were analyzed by using flow cytometer. A) Control, B) L-Arg-NI@CdSe/ZnS QDs (3 μM), and C) amonafide (25 μM); Dip G1: G0/G1 phase cells; Dip S:S phase cells; Dip G2:G2 M phase cells; apoptosis: apoptotic cells.
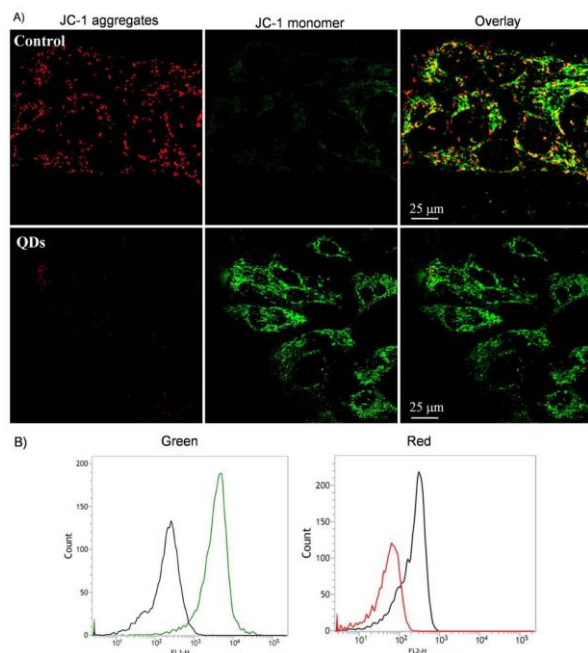

Fig. 9 A) Fluorescence images of JC-1 labeled cells taken by confocal microscopy; B) Effects of L-Arg-NI@CdSe/ZnS QDs on MMP analyzed by flow cytometry; black curve: control; green and red curve: cultures treated with QDs.

derivative-capped QDs could arrest the cell cycle at sub-G1 phase and prevent proliferation of HepG2 cells indicating its antiproliferative action and subsequent processing cell apoptosis.

6. Mitochondrial membrane potential (MMP)

Mitochondria can release proapoptotic factors, such as cytochrome C and apoptosis-inducing factor, so they play an important role in apoptosis.[36-38] Therefore, we suspected that the MMP should change due to membrane disruption. The MMP of HepG2 cells in the presence of L-Arg-NI@CdSe/ZnS QDs was measured using a MMP assay kit, in which JC-1 formed J-aggregates (red fluorescence, 590 nm) at high membrane potentials but is converted to a monomeric form (green fluorescence, 527 nm) at low membrane potentials. Fig. 9A shows the fluorescence images of JC-1 labelled HepG2 cells after QDs treatment taken by confocal microscopy. In control HepG2 cells, the obvious red JC-1 fluoresce was incorporated into cells and healthy mitochondria, indicating that the JC-1 aggregated. In the HepG2 cells treated with L-Arg-NI@CdSe/ZnS QDs, more cells with green fluorescence were observed, indicating that a disruption of membrane potential occurred. The mitochondrial collapses in apoptotic cells indicate that the reagent JC-1 no longer accumulates inside the mitochondria. Instead, it is distributed throughout the cell. The dispersed JC-1 exists in a monomeric form which fluoresces green. The quantitative analysis of JC-1-stained cells was explored by flow cytometry. Representative JC-1 red/green ratio signals recorded by flow cytometry in control cells and QDs-treated cells are shown in Fig. 9B. The quantitative analysis of JC-1-stained cells revealed a significant increase in red to green ratio in QDs-treated cells compared with control cells, which supports the fact that naphthalimide derivative-capped QDs induce HepG2 cells to undergo apoptosis.

7. ROS generation in naphthalimide derivative-capped QDs-treated HepG2 cells

As we all know, apoptosis can be triggered by increased intracellular ROS levels.[39,40] To investigate whether the mitochondrial dysfunction was mediated by the increase of ROS generation, we detected intracellular ROS level by confocal microscopy and flow cytometric method and $H_2DCF-DA$ was used as fluorescent probe. As shown in Fig. 10A, confocal microscopic analysis of $H_2DCF-DA$-stained QDs-treated cells shows significant increase in intensity of $H_2DCF-DA$ staining compared with the control cells. In other words, intracellular ROS content was significantly increased in HepG2 cells treated with QDs. To further quantify levels of intracellular ROS generation, we evaluated the ROS content inside HepG2 cells by flow cytometry. Compared with the control cells, the cells incubated with QDs showed higher fluorescent intensity (Fig. 10B), indicating higher a mounts of ROS formation in the cells. The results indicated that mitochondrial dysfunction was perhaps associated with the production of ROS. These data preliminarily suggest that ROS have an important role in naphthalimide derivative-capped QDs induced apoptosis.[41]

Conclusions

In summary, naphthalimide derivative capped-QDs with controllable sizes and strong optical emission properties, were
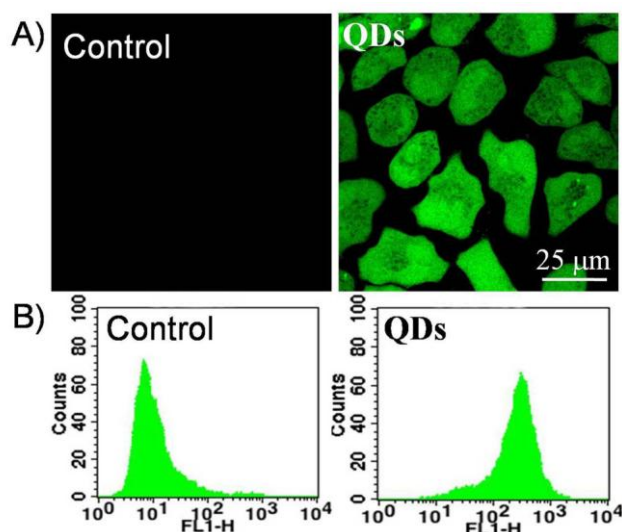
Fig. 10 Analysis of ROS production after HepG2 cells was treated with L-Arg-NI@CdSe/ZnS QDs for 6 h. The intracellular ROS level was detected by A) confocal microscope (excitation at 488 nm and emission at 530 nm) and B) flow cytometry (excitation at 488 nm and emission at 525 nm).

synthesized by capped QDs with L-Lys or L-Arg ligands and NI, linked by carboxyl groups, and inhibited the growth of multiple cancer cells more potently than amonafide. The naphthalimide derivative-capped QDs effectively inhibited the proliferation of cells due to apoptosis, which confirmed by Hoechst 33342, annexin V-FITC and JC-1 staining and MMP experiments. The cellular morphology results by TEM further confirmed the feature of apoptosis, such as shrinked nucleus, swollen and unstructured mitochondria, and condensed chromatin, etc. In the cell cycle study, QDs induced sub-G1 arrest in HepG2 cells further indicates its apoptosis action. So the QDs can efficiently induce apoptosis via a ROS mediated mitochondrial dysfunction and are more effective in promoting programmed cell death in HepG2 cells in a preliminary mechanistic study.

Acknowledgements

Notes and references

Key Laboratory of Natural Medicine and Immune Engineering, Henan University, Kaifeng 475004, China. E-mail: zhaomeixia2011@henu.edu.cn; wcjsxq@henu.edu.cn; Fax: 86-378-2864665; Tel: 86-378-2864665

† Electronic Supplementary Information (ESI) available: [details of any supplementary information available should be included here]. See DOI: 10.1039/b000000x/

1   V. Biju, *Chem. Soc. Rev.*, 2014, **43**, 744-764.
2   X. Zhang, X. Zhang, L. Tao, Z. Chi, J. Xu and Yen Wei, *J. Mater. Chem. B*, 2014, **2**, 4398-4414.
3   P. Wu and X.-P. Yan, *Chem. Soc. Rev.*, 2013, **42**, 5489-5521.
4   X. Jiang, M. Ahmed, Z. Deng and R. Narain, *Bioconjugate Chem.*, 2009, **20**, 994-1001.
5   V. Biju, T. Itoh, A. Anas, A. Sujith and M. Ishikawa, *Anal. Bioanal. Chem.*, 2008, **391**, 2469-2495.
6   R. S. Chouhan, A. Qureshi and J. H. Niazi, *J. Mater. Chem. B*, 2014, **2**, 3618-3625.
7   M. Tarantola, D. Schneider, E. Sunnick, H. Adam, S. Pierrat, C. Rosman, V. Breus, C. Sönnichsen, T. Basch, J. Wegener and A. Janshoff, *ACS Nano*, 2009, **3**, 213-222.
8   H. Sun, F. Zhang, H. Weia and B. Yang, *J. Mater. Chem. B*, 2013, **1**, 6485-6494.
9   M.-X. Zhao, H.-F. Huang, Q. Xia, L.-N. Ji and Z.-W. Mao, *J. Mater. Chem.*, 2011, **21**, 10290-10297.
10   Z. Li, Q. Sun, Y. Zhu, B. Tan, Z. P. Xu and S. X. Dou, *J. Mater. Chem. B*, 2014, **2**, 2793-2818.
11   S. Taniguchi, M. Green, S. B. Rizvi and A. Seifalian, *J. Mater. Chem.*, 2011, **21**, 2877-2882.
12   Y. Zhao, I. van Rooy, S. Hak, F. Fay, J. Tang, Cde L. Davies, M. Skobe, E. A. Fisher, A. Radu, Z. A. Fayad, C. de Mello Donegá A. Meijerink and W. J. Mulder, *ACS Nano*, 2013, **7**, 10362-10370.
13   M. Geszke-Moritz, H. Piotrowska, M. Murias, L. Balan, M. Moritz, J. Lulek and R. Schneider, *J. Mater. Chem. B*, 2013, **1**, 698-706.
14   Y. Zhang, H. Pan, P. Zhang, N. Gao, Y. Lin, Z. Luo, P. Li, C. Wang, L. Liu, D. Pang, L. Cai and Y. Ma, *Nanoscale*, 2013, **5**, 5919-5929.
15   R. Ladj, A. Bitar, M. Eissa, Y. Mugnier, R. Le Dantec, H. Fessia and A. Elaissaria, *J. Mater. Chem. B*, 2013, **1**, 1381-1396.
16   S. Banerjee, E. B. Veale, C. M. Phelan, S. A. Murphy, G. M. Tocci, L. J. Gillespie, D. O. Frimannsson, J. M. Kelly and T. Gunnlaugsson, *Chem. Soc. Rev.*, 2013, **42**, 1601-1618.
17   M. Lv and H. Xu, *Curr. Med. Chem.*, 2009, **16**, 4797-4813.
18   V. K. Malviya, P. Y. Liu, D. S. Alberts, E. A. Surwit, J. B. Craig and E. V. Hanningan, *Am. J. Clin. Oncol.*, 1992, **15**, 41-44.
19   A. Peduto, B. Pagano, C. Petronzi, A. Massa, V. Esposito, A. Virgilio, F. Paduano, F. Trapasso, F. Fiorito, S. Florio, C. Giancola, A. Galeone and R. Filosa, *Bioorg. Med. Chem.*, 2011, **9**, 6419-6429.
20   Z.-Y. Tian, S.-Q. Xie, Y.-W. Du, Y.-F. Ma, J. Zhao, W.-Y. Gao and C.-J. Wang, *Eur. J. Med. Chem.*, 2009, **44**, 393-399.
21   J. Paragas and T. W. Geisbert, *Expert Rev. Anti. Infect. Ther.*, 2006, **4**, 67-76.
22   E. Jan, S. J. Byrne, M. Cuddihy, A. M. Davies, Y. Volkov, Y. K. Gun'ko andN. A. Kotov, *ACS Nano*, 2008, **2**, 928-938.
23   D. R. Green and G. I. Evan, *Cancer Cell*, 2002, **1**, 19-30.
24   Y. H. Lee, F. Y. Cheng, H. W. Chiu, J. C. Tsai, C. Y. Fang, C. W. Chen and Y. J. Wang, *Biomaterials*, 2014, **35**, 4706-4715.
25   C. Wu, L. Shi, Q. Li, H. Jiang, M. Selke, L. Ba and X. Wang, *Chem. Res. Toxicol.*, 2010, **23**, 82-88.
26   M.-X. Zhao, J.-M. Li, L. Du, C.-P. Tan, Q. Xia, Z.-W. Mao and L.-N. Ji, *Chem. Eur. J.*, 2011, **17**, 5171-5179.
27   N. Ookubo, H. Michiue, M. Kitamatsu, M. Kamamura, T. Nishiki, I. Ohmori and H. Matsui, *Biomaterials*, 2014, **35**, 4508-4516.
28   S. Futaki, S. Goto and Y. Sugiura, *J. Mol. Recognit.*, 2003, **16**, 260.
29   X. G. Peng, M. C. Schlamp, A. V. Kadavanich and A. P. Alivisatos, *J. Am. Chem. Soc.*, 1997, **119**, 7019-7029.
30   Z. A. Peng and X. Peng, *J. Am. Chem. Soc.*, 2001, **23**, 183-184.
31   M.-X. Zhao, Q. Xia, X.-D. Feng, X.-H. Zhu, Z.-W. Mao, L.-N. Ji and K. Wang, *Biomaterials*, 2010, **31**, 4401-4408.
32   H. S. Baek, J. Y. Yoo, D. K. Rah, D. W. Han, D. H. Lee, O. H. Kwon and J.-C. Park, *Yonsei. Med. J.*, 2005, **46**, 579-583.
33   L. Mu and S. S. Feng, *J. Control Release*, 2002, **80**, 129-144.
34   J. Lovrić, H. S. Bazzi, Y. Cuie, G. R. Fortin, F. M. Winnik and D. Maysinger, *J. Mol. Med. (Berl)*, 2005, **83**, 377-385.
35   M. van Engeland, L. J. Nieland, F. C. Ramaekers, B. Schutte and C. P. Reutelingsperger, *Cytometry*, 1998, **31**, 1-9.
36   C. Borner and D. W. Andrews, *Cell Death Differ.*, 2014, **21**, 187-191.
37   R. S. Hotchkiss, A. Strasser, J. E. McDunn and P. E. Swanson, *N. Engl. J. Med.*, 2009, **361**, 1570.
38   C. X. Wang and R. J. Youle, *Annu. Rev. Genet.*, 2009, **43**, 95-118.
39   P. Li, Q. L. Zhao, L. H. Wu, P. Jawaid, Y. F. Jiao, M. Kadowaki and T. Kondo, *Apoptosis*, 2014, **19**, 1043-1053.
40   T. Ozben, *J. Pharm. Sci.*, 2007, **96**, 2181-2196.
41   M. Karlsson, T. Kurz, U. T. Brunk, S. E. Nilsson and C. I. Frennesson, *Biochem. J.*, 2010, **428**, 183-190.